Liquid crystal parameter analysis for tunable photonic bandgap fiber devices

Weirich, Johannes; Lægsgaard, Jesper; Wei, Lei; Alkeskjold, Thomas Tanggaard; Wu, Thomas X.; Wu, Shin-Tson; Bjarklev, Anders Overgaard

Published in:
Optics Express

Link to article, DOI:
10.1364/OE.18.004074

Publication date:
2010

Document Version
Publisher's PDF, also known as Version of record

Liquid crystal parameter analysis for tunable photonic bandgap fiber devices

Johannes Weirich[1], Jesper Lægsgaard[1], Lei Wei[1], Thomas Tanggaard Alkeskjold[2], Thomas X. Wu[3], Shin-Tson Wu[3] and Anders Bjarklev[1]

[1]*DTU Fotonik, Department of Photonics Engineering, Technical University of Denmark Building 345v, DK-2800 Kgs. Lyngby, Denmark*
[2]*NKT Photonics A/S, Blokken 84, 3460 Birkerød Denmark*
[3]*College of Optics and Photonics, University of Central Florida, Orlando, Florida 32816, USA*
jwei@fotonik.dtu.dk

Abstract: We investigate the tunability of splay-aligned liquid crystals for the use in solid core photonic crystal fibers. Finite element simulations are used to obtain the alignment of the liquid crystals subject to an external electric field. By means of the liquid crystal director field the optical permittivity is calculated and used in finite element mode simulations. The suitability of liquid crystal photonic bandgap fiber devices for filters, wave-plates or sensors is highly dependent on the tunability of the transmission spectrum. In this contribution we investigate how the bandgap tunability is determined by the parameters of the liquid crystals. This enables us to identify suitable liquid crystals for tunable photonic bandgap fiber devices.

OCIS codes: (060.2310) Fiber optics; (060.5295) Photonic crystal fibers; (230.3720) Liquid-crystal devices

References and links

1. P. St. J. Russell, "Photonic crystal fibers," Science **299**, 358-362 (2003).
2. A. Bjarklev, J. Broeng, and A. S. Bjarklev, "Photonic Crystal Fibres" (Kluwer Academic, Dordrecht, 2003).
3. C. Kerbage, R. S. Windeler, B. J. Eggleton, P. Mach, M. Dolinski, and J. A. Rogers, "Tunable devices based on dynamic positioning of micro-fluids in micro-structured optical fiber," Opt. Commun. **204**, 179–184 (2002).
4. T.T. Larsen, A. Bjarklev, D.S. Hermann and J. Broeng, "Optic devices based on liquid crystal photonic bandgap fibres," Opt. Express **11,** 2589–2596 (2003).
5. T.T. Alkeskjold, J. Lægsgaard, A. Bjarklev, D.S.Hermann,A.Anawati, J. Broeng, J. Li and S. Wu "All-optical modulation in dye-doped nematic liquid crystal photonic bandgap fibers," Opt. Express **12,** 5857–5871 (2004).
6. F. Du, Y. Lu and S.-T. Wu, "Electrically tunable liquid-crystal photonic crystal fiber," Appl. Phys. Lett. **85,** 2181-2183 (2004).
7. M. W. Haakestad, T. T. Alkeskjold, M. D. Nielsen, L. Scolari, J. Riishede, H. E. Engan and A. Bjarklev, "Electrically tunable photonic bandgap guidance in a liquid crystal filled photonic crystal fiber," IEEE Photon. Technol. Lett. **17**, 819-821, (2005).
8. L. Scolari,T.T.Alkeskjold,J. Riishede, A.Bjarklev,D. Hermann, A. Anawati,M. Nielsen, P. Bassi, "Continuously tunable devices based on electrical control of dual-frequency liquid crystal filled photonic bandgap fibers," Opt. Express **13** , 7483-7496 (2005).
9. A.Lorenz, H.-S. Kitzerow, A. Schwuchow, J.Kobelke, H. Bartelt, "Photonic crystal fiber with a dual-frequency addressable liquid crystal: behavior in the visible wavelength range," Opt. Express **16** 19375-19381 (2008).
10. T. R. Wolinski, K. Szaniawska, S. Ertman, P. Lesiak, A.W. Domanski, R. Dabrowski, E. Nowinowski-Kruszelnicki and J. Wojcik, "Influence of temperature and electrical fields on propagation properties of photonic liquid-crystal fibres," Meas. Sci. Technol. **17**, 985-991 (2006).
11. L. Scolari, T. T. Alkeskjold , A.O. Bjarklev "Tunable gaussian filter based on tapered liquid crystal photonic bandgap fibre," Electron. Lett. **42**, 1270-1271 (2006).

#122481 - $15.00 USD Received 12 Jan 2010; revised 8 Feb 2010; accepted 10 Feb 2010; published 16 Feb 2010

12. D. Nordegraaf, L. Scolari, J. Lægsgaard, L. Rindorf, and T. T. Alkeskjold , "Electrically and mechanically induced long period gratings in liquid crystal photonic bandgap fibers," Opt. Express **15**, 7901–7912 (2007).
13. T.T. Alkeskjold, L. Scolari, D. Noordegraaf, J.Laegsgaard, J. Weirich, L. Wei, G. Tartarini, P. Bassi, S. Gauza, S.T. Wu, A.O. Bjarklev, "Integrating liquid crystal based optical devices in photonic crystal fibers," Opt. Quantum Electron., **39** , 1009-1019 (2007).
14. L. Wei, L. Eskildsen, J. Weirich, L. Scolari, T. T. Alkeskjold, A.O. Bjarklev, "Continuously tunable all-in-fiber devices based on thermal and electrical control of negative dielectric anisotropy liquid crystal photonic bandgap fibers," Appl. Optics **48**, 497-503 (2009).
15. P.D. de Gennes, "The Physics of Liquid Crystals," (Clarendon,1974).
16. J. Weirich, J. Lægsgaard, L. Scolari, L. Wei, T.T. Alkeskjold and A.O. Bjarklev, "Biased Liquid Crystal Photonic Bandgap Fiber," Opt. Express **17**, 4442–4453 (2009).
17. J. Lægsgaard, "Modelling of a biased liquid-crystal capillary waveguide," JOSA B **23**, 1843–1851 (2006).
18. J. Li and S. T. Wu, "Extended Cauchy equations for the refractive indices of liquid crystals," J. Appl. Phys. **95**, 896–901 (2004).

1. Introduction

Photonic Crystal Fibers (PCFs) [1][2] are typically all silica optical fibers with airholes extending in the axial direction of the fiber. During the last years, a lot of research activities have been done in the field of Liquid Crystal infiltrated Photonic Crystal Fibers (LCPCFs). Due to the high optical end dielectric anisotropy and complex alignment structure of LCs, LCPCFs are a highly promising platform for tunable optical devices. Infiltrating LCs into the capillaries of a solid core PCF changes the guiding principle from modified Total Internal Reflection (m-TIR) to bandgap guiding. The optical properties of the LC infiltrated PCF and the transmission spectrum can be tuned thermally [4], optically [5] and electrically [6]-[10]. Various devices have been demonstrated, among others Gaussian filters [11] and notch filters [12], tunable polarimeters [13] and waveplates [14].

The optical mode structure in the fiber is closely linked to the mode structure in the LC infiltrated capillaries and the orientation of the LCs has a significant influence on the optical properties of the LCPCFs. The parameters of the LC together with the geometry of the capillaries and the boundary alignment determine the LC alignment. To find suitable LCs for optical devices, it is therefore of great interest to know how those parameters influence the characteristics of LCPCFs and their tunability.

For bandgap filters, sensors, waveplates and many other LCPCF devices based on electrically controlled LCs, a high tunability is desirable. In this paper, we present our simulation results to analyze the tunability of LCPCF infiltrated with various splayed aligned LCs and under the influence of an external electric field. Due to the supported complex mode structure, splayed aligned LCs allow for a continuous bandgap tunability [8][16] and are therefore of special interest. We simulate the director field distribution of LCs for a range of LC parameters using Finite Element Method (FEM) simulations. The tunability of devices based on LCPCFs is dependent on the reorientation of the LCs under an applied external electric field, and we simulate the LC realignment for various parameters. The orientation of the birefringent LCs is used to obtain the refractive index structure in the PCF capillaries. Vector element based FEM mode simulations are then applied to simulate the mode structure for a LC infiltrated capillary in the inner ring of capillaries, with and without applied bias. For these modes, we analyze the electrically induced change of effective index depending on the LC parameters. This tells us how sensitive a given LC reacts to an external electric field and allows to choose suitable LCs for applications that require a high bandgap tunability, for example Gaussian filters for optical coherence tomography or electric field sensors. It also opens up to synthesize LCs which possess properties specifically designed for a particular application.

The article is organized as follows. In section 2, we present the simulation results for the director distribution. We describe how the LC reorientation under an applied electric field de-

#122481 - $15.00 USD Received 12 Jan 2010; revised 8 Feb 2010; accepted 10 Feb 2010; published 16 Feb 2010

pends on the LC parameters. The LC alignment determines the mode structure in the capillaries of the PCF. In section 3, we show how the mode structure and tunability of a biased LCPCF depends on the LC parameters. Section 4 summarizes the results.

2. LC alignment simulations

The local orientation of a nematic LC can in general be represented by a director vector $\hat{\mathbf{n}}(x,y,z)$. It is a unit vector pointing into the direction of the rod axis of the LC molecules, as illustrated in Fig. 1b), determining the LC's local dielectric, optic and mechanic properties. We simulate the orientation of the director vector under an applied external bias, for a range of LC parameters. A schematic illustration of the investigated configuration is shown in Fig. 1a). The PCFs we consider have four rings of capillaries and are placed between two electrodes

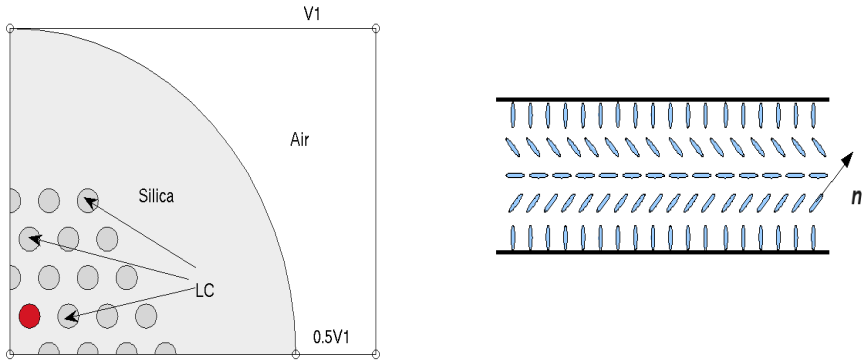

a) b)

Fig. 1. a) Schematic illustration of a photonic crystal fiber with four rings of LC infiltrated capillaries and placed between two electrodes. Symmetries are applied to reduce the calculation domain. b) Director structure for a splay aligned LC with 90° boundary alignment in a capillary.

which are on a potential V1 and grounded respectively. The capillaries are infiltrated with nematic splay aligned LCs and the PCF is surrounded by air. In the inner capillary ring in Fig. 1 we highlighted a particular capillary. The optical modes in the capillaries of the inner ring have the highest interconnection with the PBG mode. We therefore investigate the reorientation of the LCs as well as the mode structure for these capillaries. Due to symmetry there are only two capillaries in the inner ring that are not equivalent. The difference of the alignment for those two capillaries was shown to be small and hence we investigate only one of them. The general investigation of how the alignment of LCs in different capillaries of a biased LCPCF varies was done in our previous work [16]. To obtain the LC alignment, we solve Poisson's equation

$$\nabla \cdot \varepsilon \nabla \phi = 0, \tag{1}$$

and minimize the LC's free energy [15] in a self consistent procedure. We consider only two contributions, the elastic and the electric free energy, given by

$$F[\mathbf{n}] = F_0 + F_{el} = \int_\Omega d\Omega \left(\frac{K_1}{2}(\nabla \cdot \mathbf{n})^2 + \frac{K_2}{2}(\mathbf{n} \cdot \nabla \times \mathbf{n})^2 + \frac{K_3}{2}(\mathbf{n} \times \nabla \times \mathbf{n})^2 \right) - \int_\Omega d\Omega \left(\frac{1}{2}\mathbf{D} \cdot \mathbf{E} \right) \tag{2}$$

#122481 - $15.00 USD Received 12 Jan 2010; revised 8 Feb 2010; accepted 10 Feb 2010; published 16 Feb 2010

Here, K_1, K_2 and K_3 are the elastic constants of the LC. K_1 describes the energy contribution to the LC's free energy from director configurations with non-vanishing divergence also known as splay-alignment, K_2 describes twisted and K_3 bended structures. The last term in Eq. 2 is the electric free energy, with $\mathbf{D} = \varepsilon\mathbf{E}$. The dielectric permittivity tensor can be decomposed as

$$\mathbf{D} = \varepsilon_{\parallel}\mathbf{E}_{\parallel} + \varepsilon_{\perp}\mathbf{E}_{\perp} = \varepsilon_{\perp}\mathbf{E} + \Delta\varepsilon(\mathbf{E}\cdot\mathbf{n})\mathbf{n} \rightarrow \varepsilon_{ij} = \varepsilon_{\perp}\delta_{ij} + \Delta\varepsilon n_i n_j \tag{3}$$

where $\mathbf{E}_{\parallel}$ and $\mathbf{E}_{\perp}$ are the electric field components along and perpendicular to the LC rod axes, $\mathbf{n}$ is the director vector and $\Delta\varepsilon = \varepsilon_{\parallel} - \varepsilon_{\perp}$ the dielectric anisotropy. We assume hard anchoring boundary conditions, and exploit the symmetry of the problem to reduce the calculation domain to one quarter of its original size.

We choose a range of values for each of the parameters $K_1, K_3, \Delta\varepsilon$ and $\varepsilon_{\perp}$ which covers a reasonable span of commercially available LCs. Since we are dealing with nematic LCs, K_2 does not have a significant influence on the alignment and will be neglected. For each of theses parameters we simulate the LC alignment without and with applied external bias and calculate the relative alignment reorientation for the capillary in the inner ring as

$$\delta_{\hat{\mathbf{n}}} = \frac{\int\limits_{\Omega} d\Omega|\hat{\mathbf{n}} - \hat{\mathbf{n}}_{\mathbf{0}}|}{\int\limits_{\Omega} d\Omega|\hat{\mathbf{n}}_{\mathbf{R}} - \hat{\mathbf{n}}_{\mathbf{R0}}|}, \tag{4}$$

where Ω is the calculation domain, $\hat{\mathbf{n}}$ the director vector distribution with applied bias and $\hat{\mathbf{n}}_0$ the one without bias. We analyze the alignment reorientation relative to the one for a reference LC, which is represented by the director vectors $\hat{\mathbf{n}}_R$ and $\hat{\mathbf{n}}_{R0}$ with and without voltage respectively. In any of the simulations we only vary one parameter at a time, while all the others are kept fixed. As reference LC we take one with parameters similar to MDA-00-3969 (Merck, Germany) with $\varepsilon_{\perp} = 7, \Delta\varepsilon = 7$ and $(K_1, K_2, K_3) = (1.8, 1, 2.11)x10^{-11}N$. Simulations were done for both $\theta = 45^{\circ}$ and $\theta = 90^{\circ}$ boundary alignments, which are the ones we found in experiments [8] [14] and can be also be achieved by capillary coating [9]. The fiber used is a large mode area type with $d/\Lambda = 0.51$, where $d = 2.4$ is the capillary radius, and Λ the inter hole distance. The Poisson equation describing the electric field distribution and the free energy are both invariant under a spatial scaling $\mathbf{r} \rightarrow m\mathbf{r} = \mathbf{q}$, which can be seen by replacing the derivatives in Eq. 1 and Eq. 2 as

$$\frac{\partial}{\partial x_i} = \frac{\partial q_j}{\partial x_i}\frac{\partial}{\partial q_j} = m\frac{\partial}{\partial q_i}. \tag{5}$$

The scaling results in a factor m^2 in both equations which does not change the solution of the partial differential equation system. Note that the electric fields are now defined in units of the scaled system. Since we are considering PCFs with a fixed cladding diameter of $125\mu m$, we are mostly interested in a scaling of the capillary part of the fiber. In this case, the electric field distribution does change, but when keeping d/Λ constant, this effect can largely be compensated by changing the applied bias. Since we are interested in the relative tunability which depends only on the LC parameters, the strength of the external bias as well as the geometry do not influence the analysis.

From Eq. 2 and Eq. 3 we can see that the dielectric permittivity plays an important role for the reorientation of the LCs when applying an external electric field. We simulate the LC director structure for $\Delta\varepsilon \in [0, 30]$, and Fig. 2 shows the alignment reorientation depending on $\Delta\varepsilon$. Simple fitting curves show a dependence $\propto \Delta\varepsilon^{2/3}$ and $\propto \sqrt{\Delta\varepsilon}$, for 45° and 90° boundary alignment respectively. For 45° boundary alignment the electric field sees less $\varepsilon_{\parallel}$ and the electric energy density in the capillaries is therefore higher. This leads to a stronger realignment, as can be seen from the insets in Fig. 2, where the alignment deviation from the unbiased case is plotted.

#122481 - $15.00 USD Received 12 Jan 2010; revised 8 Feb 2010; accepted 10 Feb 2010; published 16 Feb 2010

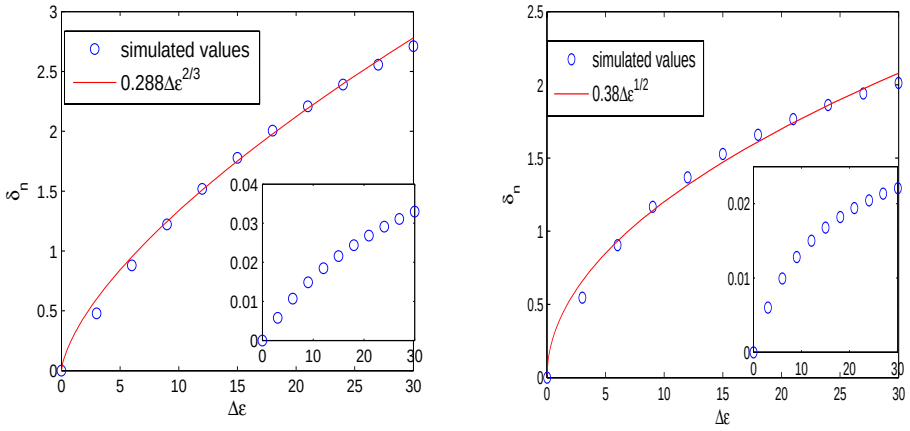

a) b)

Fig. 2. Relative alignment change when applying an external bias depending on $\Delta\varepsilon$ for a) 45° and b) 90° boundary alignment. The solid curves are the fitted values. Insets show the alignment change from the nonbiased case.

Keeping $\Delta\varepsilon$ fixed, increasing $\varepsilon_\perp$ also results in a higher average permittivity. We expect a higher $\varepsilon_\perp$ to result in a weaker electric field in the capillaries and therefore in a weaker realignment. Simulations were done for $\varepsilon_\perp \in [3,5,7,9,11,13]$. Figure 3 shows the relative alignment reorientation depending on $\varepsilon_\perp$. For both boundary alignments we obtain an alignment change

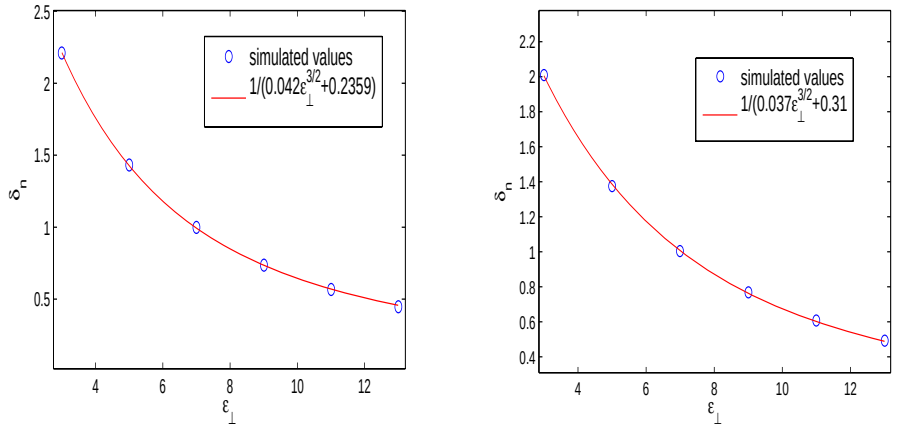

a) b)

Fig. 3. Relative alignment reorientation when applying an external bias depending on $\varepsilon_\perp$ for a) 45° and b) 90° boundary alignment. The solid curves are the fitted values. The insets show the alignment deviation from the unbiased case.

$\propto 1/(\varepsilon_\perp^{3/2} + const)$.Taking the fitted curves for the variation of $\Delta\varepsilon$ and $\varepsilon_\perp$ into account, the best tunability will be achieved by choosing a LCs with high values of $\Delta\varepsilon$, but low $\varepsilon_\perp$.

The elastic constants K_1, K_2 and K_3 describe the energy trade-off for splayed, twisted and bended configurations and we expect a weaker realignment for higher values of the K-constants.

#122481 - $15.00 USD Received 12 Jan 2010; revised 8 Feb 2010; accepted 10 Feb 2010; published 16 Feb 2010

In the following we consider the dependence of $\delta_{\hat{\mathbf{n}}}$ on K_1 with $K_3/K_1 = 1, 1.2, 1.4$. The K-constants are the only LC parameters that actually influence the LC alignment without voltage. They determine the shape of the LC distribution inside the computational domain and in this way they also influence, how much the LC will locally be affected by the electric field.

We simulate the alignment reorientation for $K_1 \in [1,4] \times [10^{-11}N]$. The results are shown in Fig. 4 For 45° boundary alignment the fitted curves are found as $\delta_{\hat{\mathbf{n}}} = 1/(0.48K_1 + 0.1), \delta_{\hat{\mathbf{n}}} =$

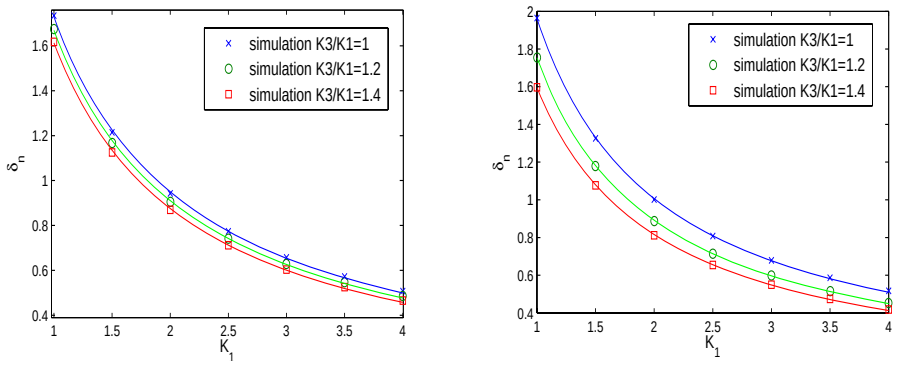

Fig. 4. Relative alignment reorientation when applying an external bias, depending on K_1 for fixed K_3 values. a) 45° boundary alignment and b) 90° boundary alignment. The smooth curves are the fitted values.

$1/(0.5K_1 + 0.1)$, and $\delta_{\hat{\mathbf{n}}} = 1/(0.52K_1 + 0.1)$ for $K3/K1 = 1, 1.2, 1.4$ respectively. The variation of the three curves is for each value of K_1 smaller than 10 percent, indicating that the influence of K_3 on the realignment is much weaker than the one of K_1. For 90° boundary alignment, the fitted curves are $\delta_{\hat{\mathbf{n}}} = 1/(0.48K_1 + 0.03), \delta_{\hat{\mathbf{n}}} = 1/(0.55K_1 + 0.02)$ and $\delta_{\hat{\mathbf{n}}} = 1/(0.6K_1 + 0.03)$ for $K3/K1 = 1, 1.2, 1.4$ respectively. We see that for perpendicular boundary aligned LCs a variation of K_3/K_1 has a stronger influence on the realignment than for 45° boundary aligned LCs. This can be explained as follows. We observe a stronger in-plane director component for higher values of K_3/K_1. The electric field sees more of $\varepsilon_{\|}$, leading to a reduced energy density and hence a weaker realignment of the LCs. This effect is is stronger for perpendicular boundary aligned LCs, resulting in a stronger relative director reorientation.

In this section, we have investigated how the LC constants influence the alignment and the reorientation when applying an external electric field. We analyzed the tunability of the LC alignment depending on the parameters $\varepsilon_{\perp}, \Delta\varepsilon$ and the K-constants.In the following we will investigate how the alignment reorientation influences the mode structure in the LC infiltrated capillaries.

3. Capillary mode analysis

The optical mode structure supported by LCPCFs is strongly connected to the alignment of the LCs in the capillaries. The positions of the bandgaps are determined by the cutoff wavelengths of the guided modes in the PCF capillaries which react very sensitively to changes in refractive index due to the reorientation of the LCs. We will now analyze how the induced effective index shift of the capillary modes depends on the LC parameters.

We use a vector element based FEM tool to solve Maxwells equations. To include material

#122481 - $15.00 USD Received 12 Jan 2010; revised 8 Feb 2010; accepted 10 Feb 2010; published 16 Feb 2010

dispersion we use the Sellmeier equation for the silica material

$$\varepsilon_{SiO_2} = 1 + \sum_{1}^{3} \frac{a_j \lambda^2}{\lambda^2 - b_j^2} \tag{6}$$

with $a = (0.6961663, 0.4079426, 0.8974794)$ and $b = (0.0684043, 0.1162414, 9.896161)$, and the Cauchy equation for the LCs [18]

$$\varepsilon_{o,e} = (A_1^{o,e} + \frac{A_2^{o,e}}{\lambda^2} + \frac{A_3^{o,e}}{\lambda^4})^2 \tag{7}$$

with $(A_1^o, A_2^o, A_3^o) = (1.47935, 0.01116, 0.00192), (A_1^e, A_2^e, A_3^e) = (1.6681, 0.01116, 0.00192)$. We set $\Delta n = 0.18875$ constant for all wavelengths in order to exclude effects of a varying birefringence on the analysis. For wavelengths in the infrared B_o, B_e and C_o, C_e have a minor influence on the slope of n_e and n_o. The assumption of a constant Δn is therefore a good approximation for the wavelength range we consider. The influence of a variation of the birefringence will explicitly be considered later on.

To quantify the bandgap tunability depending on the LC parameters, we investigate the dispersion curves of the first 6 modes in the above mentioned capillary of the first ring with and without applied bias. These modes are (in order of descending cutoff wavelength) for the 45° boundary alignment the HE_{11}, TM_{01}, HE_{21}, TE_{01} HE_{12} and HE_{31} modes. For LCs with perpendicular boundary alignment the order of the modes is HE_{11}, TM_{01}, HE_{21}, HE_{31}, HE_{12} and TE_{01}. Due to the spatially varying anisotropic refractive index in the LC capillaries, the modes differ from the ones supported by a step index fiber, but still show similar characteristic vector field structures. We therefore use the same name conventions. The mode profiles are similar for the two boundary alignments and are shown for the 45° case in fig. 5.

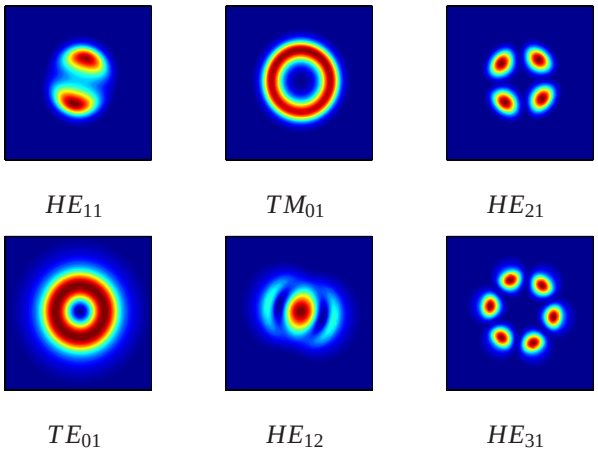

Fig. 5. Contour plot of $|\mathbf{E}|$ for the capillary modes for 45° boundary alignment.

When applying an external electric field, the two polarization directions of degenerated modes split up and the degeneracy is broken. We refer to the polarization direction which exhibits the stronger effective index shift synonymously first and y-polarization, since the external bias is applied in the y-direction, the other one second or x-polarization. To make a rigorous analysis of the bandgap tunability depending on LC parameters, one would have to simulate the photonic bandgap(PBG) mode for the whole LCPCF structure, since mode coupling and

#122481 - $15.00 USD Received 12 Jan 2010; revised 8 Feb 2010; accepted 10 Feb 2010; published 16 Feb 2010

slightly different LC alignments in different capillaries result in different dispersion curves of the capillary modes. Due to the complexity of the problem with a wide range of LC parameters we restrict ourselves to the mode structure in a single capillary. This does not allow to investigate propagation losses and the shape of the bandgaps. But in this contribution we are mainly interested in the bandgap tunability. In fact, bandgap shifts for the full transmission spectrum can be approximated very well with the cutoff wavelengths of the capillary modes when we using a capillary from the inner ring.

Figure 6 shows the effective index plots of the relevant capillary modes for a LC with $\Delta\varepsilon = 30$ (other parameters as for the reference LC), without (black, lower lines) and with (red, upper lines) applied bias for 45° and 90° boundary alignment. Here, the blue line represents the mate-

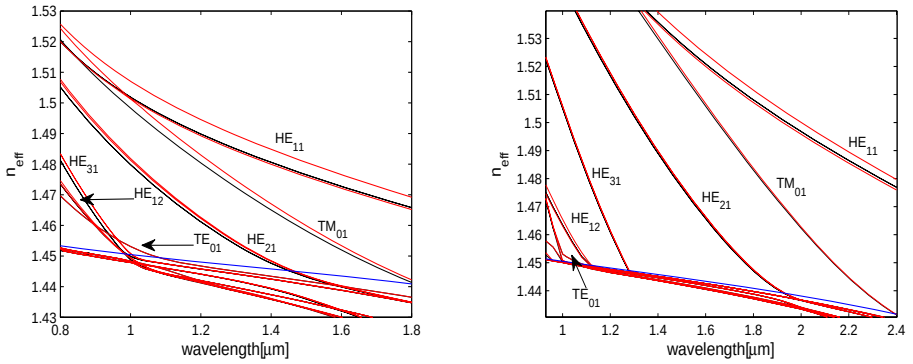

Fig. 6. Mode dispersion plots of the capillary modes for a) 45° and b) 90° boundary alignment without (black, lower) and with (red, upper) applied bias. The blue lines represent the material dispersion of the background material

rial dispersion of the background. We observe the shift in effective index as well as the splitup of degenerated modes when applying an external bias. These effects are stronger for 45° boundary aligned LCs as expected from the alignment simulations. The splitup of the two degenerated polarization directions of the HE_{11}, HE_{21}, HE_{31} and HE_{12} modes is due to the fact that only one polarization direction exhibits a strong change of the refractive index due to the reorientation of the LCs. The other polarization direction only sees a small portion of index change, which can even be negative i.e. the effective index decreases when applying a bias. Independently of the LC parameters, the TE_{01} mode shifts comparably little when applying an external electric field. This can be explained with its vector profile which is perpendicular to the LC director, as long as we have a twofold symmetry of the LC in the capillaries. This symmetry is broken by the x-component of the electric field which is weak for typical parameters and voltages. For both boundary alignments, the TM_{01} dispersion curve crosses the HE_{11} dispersion curve and becomes the mode with the highest effective index, when going to lower wavelengths. For 90° boundary alignment, the effective indices of both the HE_{31} and the HE_{12} mode is higher than the one of the TE_{01} mode. This is not the case for the 45° boundary alignment, where at the cutoff the effective index of the TE_{01} mode is higher than the one of the HE_{31} and HE_{12}.

We are now investigating the effective index shift of the modes depending on the LC parameters. Figure 7 shows the dependence of Δn_{eff} on $\Delta\varepsilon$ for a given external bias. The values for the different modes were taken close to their cutoff wavelength, since the cutoff determines the edges of the PBG. For 45° boundary alignment, the effective indices of both polarization directions of the HE_{31} mode show the highest tunability and strongest dependence on a variation

#122481 - $15.00 USD Received 12 Jan 2010; revised 8 Feb 2010; accepted 10 Feb 2010; published 16 Feb 2010

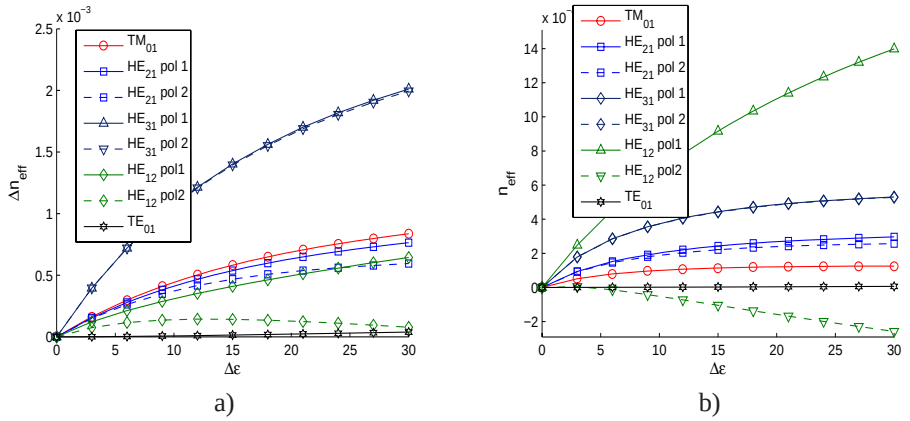

Fig. 7. Effective index shift depending on $\Delta\varepsilon$ when applying an external bias for a) 45° boundary alignment and b) 90° boundary alignment. The values were obtained close to the cutoff wavelengths of the modes.

of $\Delta\varepsilon$, followed by TM_{01} and the y-polarization direction of the HE_{21} mode. The splitup of the two polarization directions of the HE_{31} and the HE_{12} mode becomes stronger with increasing $\Delta\varepsilon$. The effective index shift of the y-polarization direction of HE_{12} increases for lower values of $\Delta\varepsilon$ and decreases for higher ones. The TE_{01} mode is affected comparably little as explained before. The y-polarization of the HE_{12} mode shows the highest tunability for perpendicular boundary alignment, followed by the two polarization directions of the HE_{31} and the HE_{21} mode. The TM_{01} mode shifts comparably little and the slope of the shift becomes more and more flat when raising $\Delta\varepsilon$. The different behavior of the TM_{01} and HE_{12} mode for the two boundary alignments can be explained as follows. 45° boundary aligned LCs reorient stronger close to the capillary boundary than LCs with perpendicular boundary alignment, since the electric field energy concentrates in areas of lower dielectric permittivity. The TM_{01} mode carries most of its energy in a ring close to the capillary boundary and sees therefore a stronger index change for 45° boundary alignment. This is the opposite for the HE_{12}, which carries most of its energy in the center of the capillary.

The analysis shows that, apart from the TE_{01} mode and the second polarization direction of the HE_{12} mode the tunability for both boundary alignments shows a qualitative similar behavior to the one we found for the director reorientation. It is therefore interesting to analyze the effective index shift of the modes relative to the one of the reference configuration. This will also tell us how much tunability we gain or loose when changing the LC parameters from the reference LC to an arbitrary LC. The results are shown in Fig. 8. For both boundary alignments, the relative effective index shift of the TM_{01}, HE_{21} and HE_{31} modes show, for lower values of $\Delta\varepsilon$, a dependence which resembles the one we found in the alignment simulations. As a comparison we plot the fitted curve found from the alignment analysis. We see that for $\Delta\varepsilon \leq 20$, with the exception of the HE_{12} mode, the relative alignment reorientation $\delta_{\hat{\mathbf{n}}}$ is well reproduced by the relative effective index shift $\Delta n_{eff,rel}$, while for higher values of $\Delta\varepsilon$ $\Delta n_{eff,rel}$ is weaker than $\delta_{\hat{\mathbf{n}}}$. For both boundary alignments, the y-polarization of the HE_{12} mode shows the strongest relative effective index change of all modes. For large values of $\Delta\varepsilon$ and 90° boundary alignment the LC reorientation focusses around the center of the capillary. This effect can also be observed, but weaker, for 45° boundary alignment, which explains the stronger relative index change of the HE_{12} mode for perpendicular boundary alignment. The TE_{01} mode and the x-polarization of the HE_{21} mode show effective index shifts which are small and qualitatively

#122481 - $15.00 USD Received 12 Jan 2010; revised 8 Feb 2010; accepted 10 Feb 2010; published 16 Feb 2010

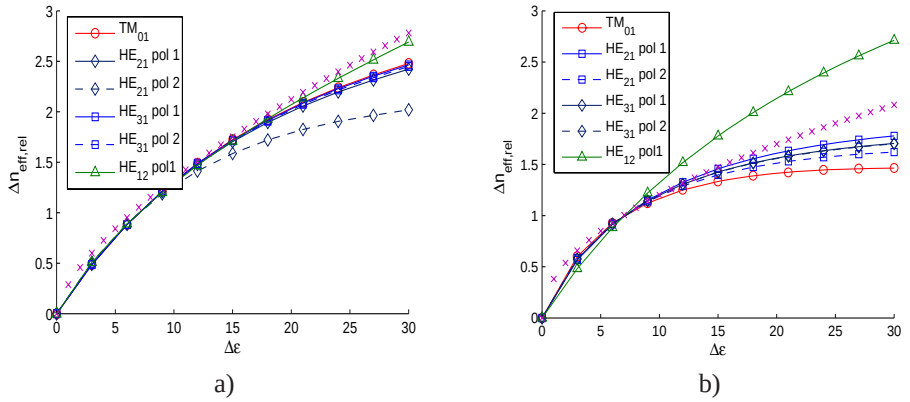

Fig. 8. Relative effective index shift depending on $\Delta\varepsilon$ for a) 45° boundary alignment and b) 90° boundary alignment. The relative values are taken with respect to the effective index shift of the modes of the reference configuration. The crossed lines show the fitting curves obtained from the alignment simulations.

different from the other modes. Since these modes are therefore not relevant for the bandgap tunability we have not plottted them in Fig. 8, and will not do so in the analysis of $\Delta n_{eff,rel}$ for the other LC parameters. The realignment of the LC over the whole capillary shows a trend for the effective index shift of the y-polarized modes, but for rigorous results, individual mode simulations have to be carried out. We will now investigate the mode structure for varying $\varepsilon_\perp$ and K-constants. The alignment simulations showed a dependence on $\varepsilon_\perp$ as $\delta\mathbf{n} \propto (\varepsilon_\perp + const)^{-3/2}$. The effective index shifts for varying $\varepsilon_\perp$ are shown in Fig. 9. We see that the strength of the

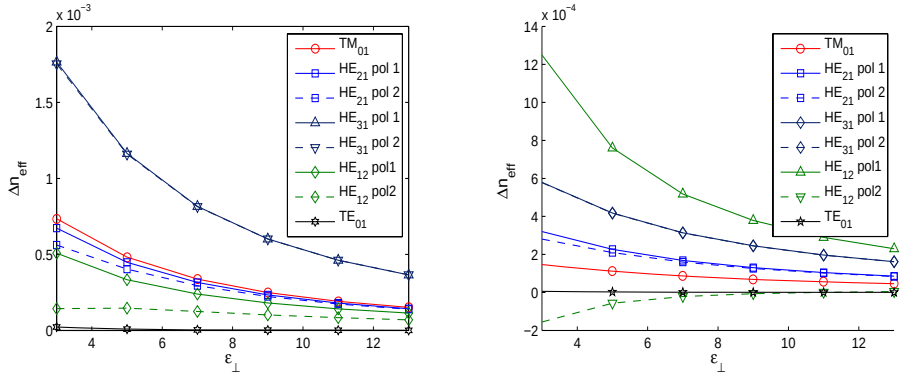

Fig. 9. Effective index shift depending on $\varepsilon_\perp$ when applying an external bias, for a) 45° and b) 90° boundary alignment. The values were taken close to the cutoff wavelengths of the modes.

effective index shift of the various modes has the same order as we found for a variation of $\Delta\varepsilon$. The relative effective shifts shown in Fig. 10 resemble the fitting curves obtained with the alignment simulations quite well. Again for perpendicular boundary alignment the HE_{12} mode shows a stronger relative tunability than the other modes. The reasons are similar to the ones for increasing increasing $\Delta\varepsilon$. For small values of $\varepsilon_\perp$, the reorientation of the LCs will be more

#122481 - $15.00 USD Received 12 Jan 2010; revised 8 Feb 2010; accepted 10 Feb 2010; published 16 Feb 2010

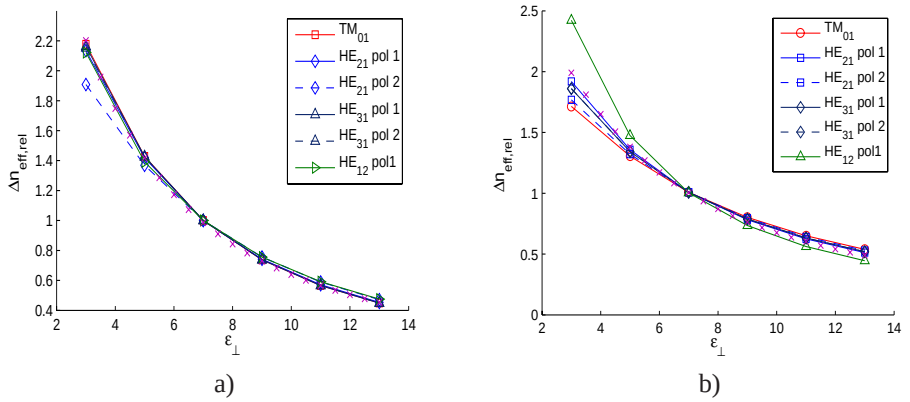

Fig. 10. Relative effective index shift depending on $\varepsilon_\perp$ for a) 45° and b) 90° boundary alignment. The relative values are taken with respect to the reference configuration. The crossed lines show the fitting curves from the alignment simulations.

and more concentrated in the center of the capillary which affects mostly the HE_{12} mode.

When varying K_3/K_1 we change the shape of the bulk alignment, even without applied external electric field. Figure 11 shows the dispersion curves for $K_3/K_1 = 1$ and $K_3/K_1 = 1.4$. For larger K_3 the effective indices increase as shown in the inset, resulting in a red-shift of the

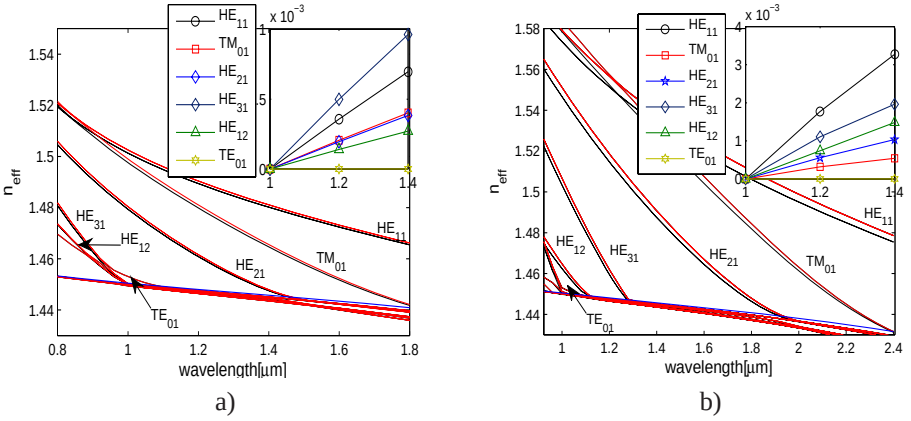

Fig. 11. Effective index plots for $K_3/K_1 = 1$ (black,lower) and $K_3/K_1 = 1.4$ (red, upper) for a) 45° boundary alignment and b) 90° boundary alignment. The insets show the effective index change of the y-polarizations of the modes depending on K_3/K_1.

modes. This can be explained with the fact, that the in-plane component of the director vector becomes larger with increasing K_3/K_1. The shift is larger in the case of 90° boundary alignment. As long as the rotational symmetry of the LC alignment is preserved, the TE_{01} mode does not shift. Therefore, the variation of K_3/K_1 does not change the dispersion curve of this mode. We now investigate the shift of effective index depending on the K-parameters when applying an external bias. Figure 12 plots Δn_{eff} depending on the K-constants. Here, the unconnected marks below the HE_{31} and above the HE_{12} modes correspond to values of $K_3/K_1 = 1.2$ and $K_3/K_1 = 1.4$ respectively. We only plot the values for these two modes in order to keep the figure clearly arranged. We see that the modes shift in the same order as observed for a variation

#122481 - $15.00 USD Received 12 Jan 2010; revised 8 Feb 2010; accepted 10 Feb 2010; published 16 Feb 2010

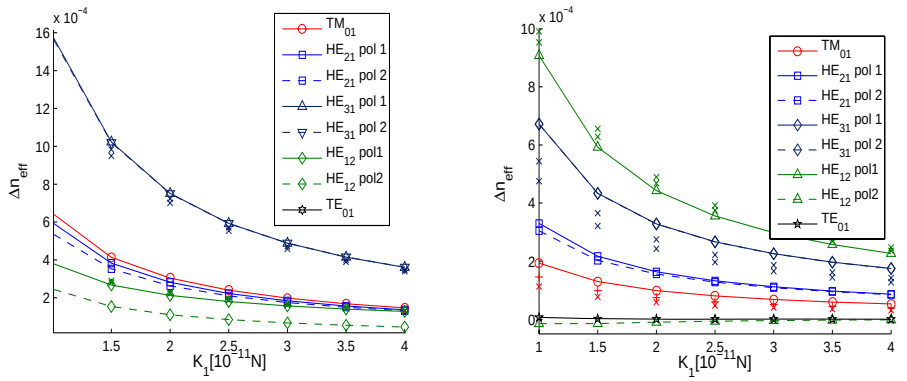

Fig. 12. Relative effective index shift depending on K_1 when applying an external bias for a) 45° and b) 90° boundary alignment.The plots show the results for $K_3/K_1 = 1$

of $\Delta\varepsilon$ and $\varepsilon_\perp$. For fixed K_1, Δn_{eff} decreases when increasing K_3/K_1 for all modes except the HE_{12} mode. This behavior for the HE_{21}, HE_{31} and TM_{01} modes can easily be explained with the weaker reorientation of the LCs for higher values of K_3/K_1. The behavior of the HE_{12} mode can be explained with the concentration of its power in the center of the capillary. For higher values of K_3/K_1 the reorientation of the LC is strongest in the center of the capillaries, and the HE_{12} mode sees therefore a stronger shift in refractive index, even though the alignment reorientation becomes weaker.

The analysis of the relative effective index shift shows that it resembles the relative alignment reorientation, which can be seen from Fig. 13. The crossed curve is the fitting result obtained

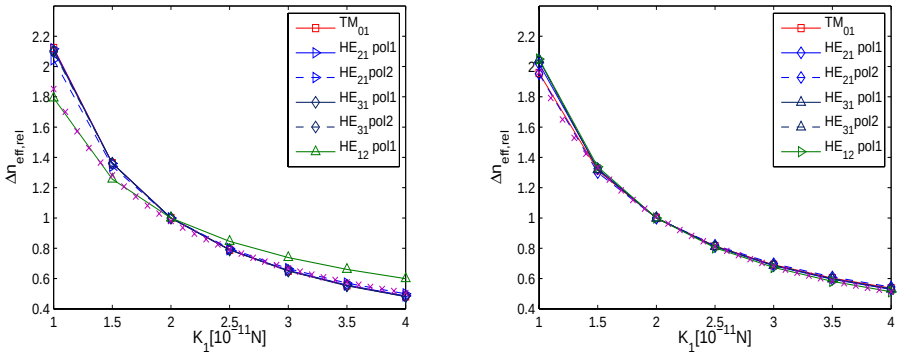

Fig. 13. Relative effective index shift depending on K_1 when applying an external bias for a) 45° and b) 90° boundary alignment. The relative values are taken with respect to the reference configuration. The crossed lines show the fitting curves from the alignment simulations. The plots show the results for $K_3/K_1 = 1$

from the alignment simulations. We see that for 45° boundary alignment the relative shift of the HE_{ml}, TE_{01} and TM_{01} mode is stronger than the one of the HE_{12}, which arises due to the stronger reorientation of the LCs towards the capillary wall and the energy concentration of the HE_{12} in the center of the capillary.

#122481 - $15.00 USD Received 12 Jan 2010; revised 8 Feb 2010; accepted 10 Feb 2010; published 16 Feb 2010

Having investigated the parameters that determine the LC alignment we found, that the relative alignment reorientation $\delta_{\hat{\mathbf{n}}}$ gives a good trend for the relative effective index shift $\Delta n_{eff,rel}$ and the tunability of the LCPCF. We are now investigating the mode behavior for different values of birefringence $\Delta n = n_e - n_o$. Figure 14 shows the relative effective index shift depending on the birefringence. Here, n_o was kept fixed while n_e was varied from $n_o + 0.05$ to

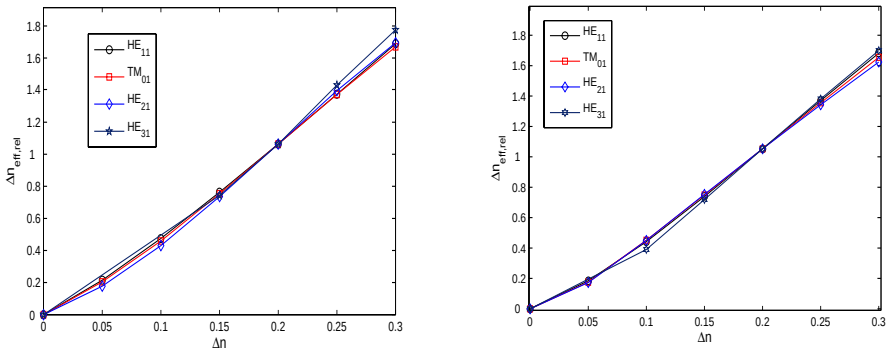

Fig. 14. Relative effective index shift depending on Δn when applying an external bias for a) 45° and b) 90° boundary alignment. The relative values are with respect to the effective index shift for the reference configuration.

$n_o + 0.3$. Since the effective indices and dispersion curves for all modes except the TE_{01} shift when changing Δn, evaluating the effective index at the cutoff wavelength of the modes does not lead to comparable results. We therefore analyze the effective index shift at one particular wavelength, $\lambda = 0.9\mu m$, relative to the effective index shift for the reference configuration at the same wavelength. We consider the wavelength range of the dispersion plots in Fig. 6 and restrict the analysis to the modes that have sufficiently many data points in this range. We see, that the relative shifts of all modes show a slightly quadratic dependence on Δn. The behavior is similar for the two boundary alignments and we expect that the different slopes for the modes is due to a different degree of confinement in the capillary. Since we obtain the effective index shift at one particular wavelength, the modes at the wavelength we investigate are unequally close to their cutoff wavelength and therefore differently well confined to the capillary.

We summarize the results of this section in table 1. The averaged relative tunability is labelled by $T45$ and $T90$, indicating the two boundary alignments. The average is taken by considering the modes in Figs. 8,10,12 and 14. The table shows the results for $K_3/K_1 = 1$. For $K_3/K_1 = 1.2$ we obtain 4% and 14% smaller values, for $K_3/K_1 = 1.4$ 8% and 22% smaller values of $T45$ and $T90$ respectively. For the parameter range investigated in this contribution, it is a very good approximation to assume that the parameters can be varied indipendently, i.e. changing the value of for example K_1 will not influence the tunability dependence on $\Delta\varepsilon$ or $\varepsilon_\perp$. Therefore we can calculate the tunability for an arbitrary LC by multiplying the tunability values for $\Delta\varepsilon$, $\varepsilon_\perp$ and K_1 from table 1. As an example we compare the LCs E7 and MDA-00-1440 from Merck, Germany with our reference LC. The physical parameters for $20°C$ are shown in table 2. By means of capillary coating with lecithin we can achieve a 90° boundary alignment. Using table 1 and the corresponding figures we can multiply the $T90$ factors for the different parameters and find a relative tunability of 2.33 and 1.92 for E7 and MDA-00-1444 respectively. The reference LC has after definition a relative tunability of 1. For devices that require high electric tunability the use of E7 would therefore be advantageous.

#122481 - $15.00 USD Received 12 Jan 2010; revised 8 Feb 2010; accepted 10 Feb 2010; published 16 Feb 2010

Table 1. Average mode tunability for 45° and 90° boundary aligned LCs.

$\Delta\varepsilon$	$T45$	$T90$	$\varepsilon_\perp$	$T45$	$T90$	K_1	$T45$	$T90$	Δn	$T45$	$T90$
3	0.51	0.57	3	2.11	1.92	1	2	2.02	0.05	0.21	0.18
6	0.89	0.92	5	1.41	1.35	1.5	1.31	1.32	0.1	0.5	0.44
12	1.47	1.34	7	1	1	2	0.98	1.01	0.15	0.74	0.74
18	1.89	1.57	9	0.74	0.78	2.5	0.81	0.81	0.2	1.06	1.05
24	2.19	1.73	11	0.57	0.62	3	0.65	0.69	0.25	1.39	1.37
30	2.42	1.83	13	0.46	0.51	4	0.49	0.54	0.3	1.71	1.67

Table 2. The physical parameters of E7 and MDA-00-1444

	$\Delta\varepsilon$	$\varepsilon_\perp$	K_1	K_3/K_1	Δn
$E7$	12.65	5.13	1.34	1.2	0.205
$MDA-00-1444$	29.47	7.01	1.44	1.09	0.165

4. Conclusion

We analyzed the reorientation of LCs in a PCF due to an applied external bias for a range of LC parameters. Using fitting curves, we found approximations on how the electrically induced alignment change depends on the LC parameters. We showed, that 45° boundary aligned LCs reorient stronger than perpendicular aligned ones, due to their lower average dielectric permittivity. We investigated how the LC reorientation affects the tunability of the capillary modes. The analysis of the 6 lowest order modes shows, that in most of the cases the relative effective index shift resembles the relative alignment change very well. We found that the tunability is proportional to $\Delta\varepsilon^{2/3}$ and $\Delta\varepsilon^{1/2}$ for 45° and 90° boundary alignment respectively. For both boundary alignments the tunability depending on $\varepsilon_\perp$ is $\propto (\varepsilon_\perp^{3/2} + const)^{-1}$ and for K_1 we found a relation as $\propto (K_1 + const)^{-1}$. We also investigated the relative effective index shift depending on the birefringence and found a slightly quadratic dependence. The analysis tells us how much tunability we will gain when changing the LC parameters from a reference configuration to the ones of another LC. Different LCs can be compared and the one with the highest tunability can be determined. This helps for selecting suitable LCs for LCPCF devices.

#122481 - $15.00 USD Received 12 Jan 2010; revised 8 Feb 2010; accepted 10 Feb 2010; published 16 Feb 2010